Inspection of contamination in nitrogen plasmas by monitoring the temporal evolution of the UV bands of NO-γ and of the fourth positive system of N 2

O. Carrivain, R. Hugon, G. Marcos, C. Noël, O. Skiba, T. Czerwiec

Inspection of contamination in nitrogen plasmas by monitoring the temporal evolution of the UV bands of NO-γ and of the fourth positive system of N_2

O.Carrivain[1,2], R. Hugon[2,a], G. Marcos[2,3], C.Noël[2], O.Skiba[1], and T.Czerwiec[2,3]

[1] Institut de Recherche Technologique Matériaux Métallurgie et Procédés (IRT-M2P), 4 rue Augustin Fresnel, Metz, France

[2] Université de Lorraine, Institut Jean Lamour (IJL), UMR CNRS 7198, Campus ARTEM, allée Andrée Guinier, BP 50840, F-54000, Nancy, France

[3] Université de Lorraine, Laboratory of Excellence Design of Alloy Metals for Low-Mass Structures (Labex DAMAS), 7 rue Félix Savart, F-57070 Metz, France

a) Author to whom correspondence should be addressed: robert.hugon@univ-lorraine.fr

Abstract

In this study, contamination by oxygen species in nitrogen plasmas produced by the active screen system used for plasma nitriding (ASPN) has been investigated by optical emission spectroscopy in the spectral range of 200-900 nm. Temporal evolution of emission intensity of different species (N_2, N_2^+, NO, OH, H, NH and Fe) was monitored, as well as electrical characteristics (current and voltage) of the discharge produced by pulsed unipolar power supply. In nitrogen plasma, it was found that the emission of oxygen containing species (NO and OH) decrease with time, while Fe emission intensity increases. Such behavior is observed only when the discharge is initiated immediately after venting the reactor. Starting from the hypothesis of a contamination of the reactor walls by water vapour, we propose an explanation based on a synergistic effect between the temperature and the reactive nitrogen created by the plasma. Such a long decay of NO emission was not observed in N_2-H_2 gas mixtures. After decontamination, the fourth positive system of N_2 could be observed. Such a

not commonly observed system can be used as a tool to control reactor cleanness in pure nitrogen discharge for nitriding applications.

Keywords

Optical emission spectroscopy, nitriding process, wall desorption, contamination, fourth positive system of nitrogen.

1. Introduction

Plasma processes are among the promising nitrogen fixation processes,[1-2] especially in nanomaterials.[3] Plasma-assisted nitriding (PAN) is one of such plasma-assisted technology.[3] PAN is widely used in industry to improve the surface properties of steels,[4] it is also an attractive way to increase the durability of textured steels[5]. PAN treatments are mainly carried out using pulsed DC discharges in diode configuration at moderate pressure (1-10 mbar).[6] In this configuration (also known as DCPN, direct current plasma nitriding), the components to be treated serve as a cathode and the chamber wall as an anode. The reactivity of the plasma is coupled to the heating of the substrate because a sheath forms around the cathode and the adjustment of the bias voltage allows the control of the energy of the incident ions. The bombardment of the cathode makes it possible to adjust the temperature of the parts to be treated, which is a crucial parameter in nitriding. The bombardment of the samples by ions from the plasma is associated to detrimental sputtering of the part to be treated, but proves to be an asset in limiting the oxidation of the surfaces.

In transferred plasma nitriding processes,[6] plasma generation is decoupled from the surface of the substrate. Such a situation is realized in the active screen plasma nitriding (ASPN) process[7-11] we are studying here. This relative new technology developed by George[8] overcomes inherent limitations of DCPN (arcing, edging effect, and overheating due to the

hollow cathode effect) leading to surface damage and non-uniform nitriding. Such a process opens the way to promising industrial applications. In this configuration, a metal mesh screen surrounding the parts to be treated serves as a cathode and the chamber wall as an anode. As in DCPN, ASPN works under primary vacuum (0.3 to 12 mbar).[12-15] In ASPN, the surface of the metallic mesh is subjected to intensive ion bombardment and sputtered metallic species are deposited on the reactor walls. Metals can gettered water vapour during the opening of the reactor.[16,17] Due to the high temperature reached by the metallic meshes during nitriding, these components are nitrided, especially if they are composed of steel.[18] Optical emission spectroscopy (OES) is a powerful tool to investigate electrical discharge for plasma processing.[19] In plasma nitriding, OES is often used in the range of 300-900 nm in order to identify the active species[20-24] and which gas composition (i.e. N_2/H_2 ratio) achieves the best nitriding results.[23, 24]

During a nitriding treatment of steels, species containing nitrogen in active form (atomic nitrogen, excited nitrogen molecules, NHx radicals, etc.) adsorb onto surfaces and atomic nitrogen can thus diffuse into the steels.[25] These steps, still relatively little described in the literature, are very sensitive to the oxidizing state of the extreme surface. Following these steps, a solid solution of nitrogen or nitrides may form depending on the type of treated steels. Cleaning step is necessary in order to eliminate the superficial oxide layer that can be found on the surface of steels, particularly on stainless steels. In ASPN/DCPN, ionic bombardment is used to ensure this cleanness. As a matter of fact, when a nitriding reactor is open to place the samples to be treated, contaminants containing oxygen (water vapor and hydrocarbon) are adsorbed on the walls of the reactor. The desorption of the oxygen species liable to contaminate the surface of the parts to be nitrided will depend on many parameters, the main ones being the residence time, the temperature and the size of the reactor.

The purpose of this paper is to study this critical aspect of the ASPN process. Cleaning step is an important phase of the nitriding treatment. This paper is devoted to spectroscopic investigation of oxygen contamination. Nevertheless, oxygen lines are not observed in our conditions. For this reason, we propose to follow temporal evolution of NO-γ in spectral range of 200-300 nm, as tracer of oxygen contamination.

2. Materials and Method

2.1 Plasma reactor and pulsed DC power supply

Experiments have been conducted in an Active Screen Plasma Nitriding (ASPN) reactor described in Fig. 1. It consists of a cylindric stainless steel chamber of 460 mm in diameter and 360 mm in height. The cathode is a stainless steel (AISI 304 L) cylindric mesh screen of 340 mm in diameter and 220 mm in heigth placed in the center of the reactor and surrounding by a worktable (Ø = 24 cm) where samples to be nitrided are placed. The mesh size is 20×10mm and the thickness is 2 mm. The inter-electrode distance (distance between active screen and wall reactor) is equal to 6 cm. In order to avoid an overheating of the wall-reactor, a water cooling system permits to reduced the temperature.

FIG. 1. Experimental set-up

The cathodic screen is connected to a DC-pulse generator (SAIREM, V_{max} = 700 V, I_{max} = 3 A) with adjustable frequency (1 to 10 kHz) and a variable duty cycle. At the generator output, a charge resistance (81 Ω) was used to maintain a stable working point. Temporal evolution of the discharge current and voltage were measured as close as possible to the cathode with a Hall effect current probe (1147 A, Agilent, sensibility 0.1 V/A, 50 MHz bandpass) and voltage probe (N2771A, Agilent, High Voltage Probe 1000:1, 30 kV, 50 MHz

bandpass), respectively. Typical electric discharge caracteristics are depicted in Fig. 2. At the discharge ignition, current present peaks and tends to a constant value. Thereafter, we will only give the average value of current and voltage during t_{on} (between 300 and 500 µs) to facilitate their analysis. Temporal evolutions presented in the following section will be of a few hundred minutes, wich represents the typical duration of a nitriding process.

FIG. 2. Temporal evolution of discharge current (a) and voltage discharge (b) in a nitrogen plasma at 0.5 mbar.

The precursor gas (N_2 and H_2) are injected from the top of the reactor. The purety of gas is 99.999 % for N_2 and 99.9999 % for H_2. Gas flow rates are regulated using mass flow controlers (Air Liquide, RDM-280). Total flow rate is fixed to 100 sccm. The pressure inside the reactor is regulated by a rolling valve upstream a 60 m^3/h rotary pump and measured by a capacitive pressure sensor (LEYBOLD, CERAVAC CTR 100, pressure range 1.3×10^{-3} to 13 mbar). The limit vacuum is 7×10^{-3} mbar. The gas residence time was estimated to 20 s. The temperature is measured by means of a type K thermocouple inserted in a metallic sample placed on the worktable in the center of the reactor.

2.2 Optical Emission spectroscopy

Active screen plasma emission is recorded through a quartz windows in order to measure spectra in the range of 200-900 nm. Two configurations are employed. In configuration 1, an optical fiber (OceanOptics, P50-2-UV-VIS) was used and plasma emission was imaged into the entrance slit of an echelle spectrometer (ANDOR, mechelle 5000) coupled to an ICCD detector (iStar DH734). The exposure time was 50 ms with 100 accumulations. The spectral resolution is 0.1 nm at 500 nm. With this spectrometer, the whole spectrum is recorded at one time. In configuration 2, plasma emission was collected by an optical fiber (P600-2-SR,

OceanOptics) with a transmission higher than 60 % in the spectral range of 200-900 nm, and imaged into the entrance slit of a monochromator (TRIAX-550, Jobin-Yvon) coupled to an ICCD detetector (Horiba i-Spectrum Two). The slit aperture was fixed to 50 µm. The grating of the monochromator is blazed at 300 nm with 1800 grooves/mm. The dispersed light is recorded by means of a 16-bit intensified CCD with an intensifier gate width fixed to 50 ms and 200 accumulations. The spectral resolution of our system (spectrograph+ICCD) is 0.03 nm/pixel, wich allows to distinguish the rotational structure of the first negative system of N_2^+. Configuration 1 was dedicated to monitor the temporal evolution of emitting species (N_2, N_2^+, NH…) in the spectral range of 200-900 nm with a temporal resolution around 1 min and a low sensitivity. The second configuration was used to monitor the temporal evolution of NO between 242-262 nm with a higher sensitivity and spectral resolution.

2.3 Experimental approch

Contamination of the plasma by oxygen-containing species during nitriding treatment was studied by following the plasma emission in a wide spectral range (200-900 nm), and measuring the electrical characteristics of the discharge. The inside of the reactor was exposed to ambient air during about 30 min.; the relative humidity of the experimental room was about 40 %. Then, the reactor was closed and pumped down to a pressure of 3×10^{-2} mbar. Finally, the reactor was filled with nitrogen and the power supply was turned on to switch on the plasma. The applied voltage output was fixed to -600 V. The duration of the discharge and post-discharge were t_{on} = 570 µs and t_{off} = 150 µs ($f \approx 1.4$ kHz), respectively.

3. Results

OES spectra measured in pure nitrogen at 0.5 mbar are presented in Fig. 3. The foremost observed transitions are presented in Table I. Three main categories of species can be identified:

(1) Species related to the injected gas: N_2, N_2^+, N and N^+. OES spectra are dominated by the $B^2\Sigma_u^+ \rightarrow X^2\Sigma_g^+$ system (First Negative System, FNS) of N_2^+ and the $C^3\Pi_u \rightarrow B^3\Pi_g$ system (Second Positive System, SPS) of N_2. The progression v' = 0-3 of the second positive system and v' = 0-1 for first negative system are observed. Some atomic lines of N and N^+ are also observed;

(2) Species attributed to reactor contamination: NO, OH, NH and H. Reactor contamination can originate from micro-leak, wall desorption or the use of unclean gas. Progression v' = 0-1 of NO-γ ($A^2\Sigma^+$-$X^2\Pi$) are observed. The electronic transition $A^3\Pi(0)$-$X^3\Sigma^+(0)$ of NH and $A^2\Sigma^+(0)$-$X^2\Pi(0)$ of OH and H lines (H_α, H_β and H_γ) are also identified. Please note that no oxygen lines can be observed;

(3) Species related to the sputtering of the active screen mainly caused by nitrogen ions bombardment: Fe and Fe^+.

FIG. 3. Emission spectrum of N_2 discharge in the range of 200-900 nm (a) and 200-400nm (b). The spectra were recorded at the beginning of the discharge (after venting).

Species	Transition	Line position (nm)	Emission system
Fe	$x^5F^0(5) \rightarrow a^5D(4)$	248.327	
Fe^+	$Z^6D^0(9/2) \rightarrow a^6D(9/2)$	259.94	
H_γ **H_β** **H_α**	n=5→n=2 n=4→n=2 n=3→n=2	434.05 486.13 656.62	Balmer
N	$^4P^0(1/2) \rightarrow {}^4P(1/2)$ $^4P^0(3/2) \rightarrow {}^4P(3/2)$ $^4P^0(5/2) \rightarrow {}^4P(5/2)$ $^4P^0(1/2) \rightarrow {}^4P(3/2)$	820.036 821.072 821.65 822.314	
N^+	$^3F^0(3) \rightarrow {}^3D(2)$ $^3F^0(4) \rightarrow {}^3D(3)$	500.15 500.51	
N_2^+	$B^2\Sigma_u^+(v'=0) \rightarrow X^2\Sigma_g^+(v''=0)$	391.44	First negative system
N_2	$C^3\Pi_u(v'=0) \rightarrow B^3\Pi_g(v''=2)$ $D^3\Sigma_u^+(v'=0) \rightarrow B^3\Pi_g(v''=0)$ $D^3\Sigma_u^+(v'=0) \rightarrow B^3\Pi_g(v''=1)$ $D^3\Sigma_u^+(v'=0) \rightarrow B^3\Pi_g(v''=2)$ $D^3\Sigma_u^+(v'=0) \rightarrow B^3\Pi_g(v''=3)$	380.49 225.71 234.75 244.40 254.66	Second positive system Fourth positive system

	$D^3\Sigma_u^+(v'=0)\rightarrow B^3\Pi_g(v''=4)$ $D^3\Sigma_u^+(v'=0)\rightarrow B^3\Pi_g(v''=5)$ $D^3\Sigma_u^+(v'=0)\rightarrow B^3\Pi_g(v''=6)$	265.58 277.28 289.81	
NH	$A^3\Pi(v'=0)\rightarrow X^3\Sigma^+(v''=0)$	336.01	
OH	$A^2\Sigma^+(v'=0)\rightarrow X^2\Pi(v''=0)$	306.36	Angstrom system
NO	$A^2\Sigma^+(v'=0)\rightarrow X^2\Pi(v''=2)$	247.87	γ system

TABLE I. List of the most intense transitions observed in the screen plasma by OES.

The temporal behavior of N_2 and N_2^+ peaks intensities are depicted in Fig. 4(a) and appeared to be correlated to the electrical characteristics (Fig. 5(a)) rather than to the substrate temperature (Fig. 5(b)). Between 0 and 40 min., emission intensities of both species rapidly decrease and slightly afterwards. Characteristic time of both species are closed to 10 min. N_2 and N_2^+ emission intensity remains constant for time higher than 100 min. Time evolutions for N and N+, not shown here, are similar.

FIG. 4. Temporal evolution of the emission intensity of the N_2^+-(0,0) band of the FNS (blue circle) and of N_2-(0,2) band of the SPS (black square) (a) and NO-γ(0,2) band and OH (b) and H_α and NH (c). The spectra were recorded at the beginning of the discharge (after venting).

The temporal evolution of emission intensity of NO γ-band (0,2) and OH ($A^2\Sigma^+(0)$-$X^2\Pi(0)$ band) are depicted in Fig. 4(b). It shows that NO and OH emissions have different dynamics. Indeed, OH emission rapidly decreases with time, whereas NO emission intensity remains constant during the first 35 min. and then decreases when the temperature inside the reactor (measured at center of the reactor) becomes higher than 100 °C. The curve fitting with a single exponential decay function of NO* and OH* temporal behavior gives a characteristic time of 57 and 50 min. respectively. The fact that NO* and OH* emission intensity are still observable for long times is probably due to a micro leak. The leakage rate was estimated to 0.06 sccm.

The emission intensity evolutions as a function of time from the starting of the discharge are presented for NH* and H_α in Fig. 4(c). NH emission increases up to 125 min. and remains

relatively constant afterward. H was found to decrease with a characteristic time close to 50 min.

Temporal behaviors of emission intensity of iron species (Fe and Fe^+) are also investigated (cf. Fig. 6). It was found that emission of Fe and Fe^+ (not shown here) seems correlated to the NO temporal behavior. Indeed, iron species emission increase up to 250 min. when NO decreases, and remain constant afterward.

FIG. 5. Temporal evolution of the current and voltage discharge (a) and temperature measured at the center of the reactor (b).

FIG. 6. Temporal evolution of the emission intensity of Fe and NO-γ(0,2). The spectra were recorded at the beginning of the discharge (after venting).

The emission spectra recorded between 242-262 nm are presented in Fig. 7(a) and 7(b), respectively 50 min. and 340 min. after the beginning of the discharge. The spectrum measured at 50 min. consists of the NO-γ bands and it is challenging to detect iron lines (Fig. 7(a)). Over time, NO-γ emission bands decrease. The N_2 fourth positive system ($D^3\Sigma_u^+$-$B^3\Pi_g$) is clearly observable but strongly interferes with NO-γ emission. This system is easier to be observed only after 200 min. In our knowledge, only a few observations of the fourth positive system of N_2 has been already reported in radiofrequency[26] and microwave discharge[26,27] around 10 mbar. However, no spectrum is shown in these papers. This system is observed but only the v' = 0 progression as already reported by Filippelli et al.[28] in electron-impact excitation measurements. However, the v' = 1-3 levels have been observed by high-resolution near-infrared diode laser absorption spectroscopy through the $E^3\Sigma_g^+$(v'' = 1-3) states.[29] It must be noted that the spectral resolution of our system does not allow to resolve the rotational structure of the fourth positive system, because each band is composed of five principal heads closely spaced.[30]

If the nitrogen plasma is switched off once the transient decontamination regime has passed, it is again possible to observe the fourth positive of nitrogen if a nitrogen plasma switched on again. This remains valid as long as the reactor is not opened.

FIG. 7. Emission spectra of nitrogen plasma in the spectral range of 242-262 nm under unclean (a) and clean (b) condition at 0.5 mbar.

After opening the reactor to air, emission spectra were measured between 242 and 262 nm for a gas mixture composed of 80% N_2-20% H_2. Same voltage (- 600 V) and total pressure (0.5 mbar) as in the case of pure nitrogen were used (Fig. 8). Fig. 8(a) presents emission spectra recorded at the early beginning of discharge and 10 min. after the beginning of the discharge. The temporal evolution of NO intensity is presented in Fig. 8(b). By contrast to the case of pure nitrogen plasma, fourth positive system appears at the beginning of the discharge and rapidly decreases (after 6 min). When hydrogen was removed after 90 min (pure nitrogen discharge), emission bands of NO appear and decrease with a very long characteristic time (75 min). This observation proves that the reactor was not clean at the beginning of the discharge; Hydrogen probably prevents NO production, and so it is impossible to conclude on the contamination state of the reactor.

FIG. 8. (a) Emission spectra recorded in the range of 242-262 nm for gas mixture composed of 80 % N_2- 20 % H_2 at 0.5 mbar. The spectra were recorded at the beginning of the discharge (after venting). (b) Temporal evolution of NO-γ(0,2) band intensity in 80 % N_2- 20 % H_2 plasma following by pure nitrogen discharge without venting.

4. Discussion

4.1 Contamination of nitrogen plasmas

The walls of the reactor as well as the grid are made of stainless steel and it is known that water vapor adsorbs therein at ambient temperature when the reactor is vented to air.[16,17] Once

under vacuum, the main species that desorb from stainless steels are H_2, H_2O and CO.[16,17] The desorption rate of these species depends on a large number of parameters, the main ones being the pressure, the pumping speed in the reactor and the temperature of the surfaces. Studies concerning the desorption of water vapor on stainless steels show that there are different types of adsorption sites associated to different activation energies. At room temperature, there are mainly two types of adsorption sites. The first has a low activation energy (0.3 eV) and leads to desorption of H_2 controlled by the slow diffusion of hydrogen atoms inside stainless steel.[31] The second are chemisorption sites associated to much higher activation energies: 1.4 eV for Ishikawa et al.[31] and 2 eV for Joly et al.[32]. On these sites, hydroxyl groups would be chemisorbed which would give water vapor on desorbing. Thus, for temperatures below 250 °C, it is hydrogen which is the predominant species during desorption, while it is water vapor and carbon monoxide which are the predominant species for higher temperatures.[31] The influence of plasmas on the outgassing of stainless steels is not well documented.[16,17] Shin et al.[17] have shown that treatment with atomic hydrogen makes it possible to reduce the outgassing of H_2O and CO. Itho et al.[16] have shown that treatment with argon plasma makes it possible to greatly decrease the quantity of H_2O desorbed but increases the quantity of H_2 in the reactor. They explain this production of H_2 by the dissociation of water vapor in the argon plasma. Such hydrogen outgassing has been observed in a titanium deposition process operating under a primary vacuum in a large volume stainless steel reactor (0.14 m^3).[33] In argon plasma, the only contaminant detected by OES is hydrogen (via the H_α line).[33] Depending on the power applied to the cathode, it takes between 100 and 300 min. to no longer observe this line in the plasma. It is interesting to note that our observations are very reproducible whatever the opening time of the reactor (from 30 min. to several hours).[33]

It is not easy to estimate the temperature of the wall as well as that of the grids. However, we can assume that the temperature measured on a substrate placed at the center of the reactor

is close to those of the walls. For the screen, it can be estimated to be above 500 °C with reference to the temperature of the cathodes subjected to similar voltages and currents in the DCPN processes. Based on the literature data for outgassing mechanisms under the influence of temperature, we can assume that hydrogen and water vapor desorb from the grids while the walls would only be the source of hydrogen. The decrease in the intensity of the emission lines of species containing only nitrogen is mainly explained by the strong variations in the electrical parameters during this step. Indeed, during this first period (cf. Fig. 4), the composition of the gas varies enormously because of the slowness of the degassing which results from the thermal equilibrium of the reactor. However, thermal outgassing cannot fully explain our experimental results. Indeed, hydrogen lines emission are continuously decreasing whereas it should increase at least at the beginning of the desorption process as observed by Czerwiec et al.[33]. It is interesting to note that the NH line intensity firstly increases. Hence some reactive nitrogen species like N, vibrationally excited species $N_2(v)$ or metastable states od N_2 must be probably involved in surface reactions with the OH radicals resulting from the adsorption of water on stainless steel. Such surface reactions would be able to produce NO and NH from the water vapor absorbed on the wall or on the screen.

The continuous increase in iron emission during the first three stages leads us to believe that the preponderant surface in these surface reactions must be the grid itself. It is indeed from the grid that the iron atoms are sputtered. It is very probable that oxides form at the surface of the active screen, thus limiting the iron sputtering efficiency. As the possibility to observe the fourth positive system of N_2, obtaining stable iron emission over time could be a potential indicator of cleanliness of the reactor.

One very important thing that should not be forgotten is the fact the discharge is periodically cut off. In plasma nitriding processes, pulsed unipolar power supply allows a periodic cutting of the discharge in order to prevent electric arcs from developing. Long duration arcs can

deteriorate the active screen in the ASPN process. Active nitrogen species can react on surfaces with adsorbed oxygen species only during the part of the cycle during which voltage is applied to the active screen. In the temporal post-discharge (t_{off}), the active nitrogen species disappear quite quickly during this period and no longer react with the species adsorbed on the surfaces. The time for this cut-off is short enough not to have any influence on the temperature of the walls and the screen. Thus, the thermal desorption of the species containing oxygen and hydrogen continues during the cut-off period. The reactivation of the plasma therefore takes place in a polluted atmosphere at the end of each electrical cycle.

4.2 The $D^3\Sigma_u^+$ state of N_2: observations and population mechanisms

As presented before, fourth positive system seems to be correlated to the reactor cleanness, by contrast to the emission bands of NO, which are clearly linked to reactor contamination. During the decontamination phase, the decrease of NO emission intensity reveals the fourth positive system. At this moment, it could be interesting to study the population mechanisms of both excited species (NO and N_2).

In this case of NO emission, it could be suppose that NO excited state ($A^2\Sigma^+$ at about 5.5 eV) is produced by direct electronic impact. Electrical characteristics (cf. Fig. 5a) are relatively constants; it can be assume that emission intensity is proportional to the NO concentration.

FIG. 9. Potential energy curves for $X^1\Sigma_g^+$, $A^3\Sigma_u^+$, $B^3\Pi_g$, $C^3\Pi_u$ and $D^3\Sigma_u^+$ states of N_2. Potential curves are calculated assuming Morse potential and by using spectroscopic constants given by Lofthus and Krupenie [31] for $X^1\Sigma_g^+$, $A^3\Sigma_u^+$, $B^3\Pi_g$, $C^3\Pi_u$ and by Lewis et al. for $D^3\Sigma_u^+$ [30].

For the case of the fourth positive system, population mechanisms remain relatively unknown. Fig. 9 presents the potential energy curves of N_2 electronic state observed in ASPN-plasma. Potential curves are calculated assuming Morse potential and by using spectroscopic constants given by Lofthus and Krupenie[30] for $X^1\Sigma_g^+$, $A^3\Sigma_u^+$, $B^3\Pi_g$, $C^3\Pi_u$ and by

Lewis et al. for $D^3\Sigma_u^+$.[29] $D^3\Sigma_u^+$ is shown in dashed line, because potential curve is not well known. As depicted in Fig. 9, this state requires 14 eV to be populated from the ground state. The origin of populating the $D^3\Sigma_u^+$ state ask question. Several mechanisms can be considered such as, excitation by electronic impact from the fundamental state (R1), and from the metastable state $A^3\Sigma_u^+$ (R2), and by pooling reaction (R3).

$$N_2\left(X^1\Sigma_g^+\right) + e \rightarrow N_2(D^3\Sigma_u^+) \quad \text{(R1)}$$

$$N_2(A^3\Sigma_u^+) + e \rightarrow N_2(D^3\Sigma_u^+) \quad \text{(R2)}$$

$$N_2(A^3\Sigma_u^+) + N_2(A^3\Sigma_u^+) \rightarrow N_2(D^3\Sigma_u^+) \quad \text{(R3)}$$

The production of $N_2(D^3\Sigma_u^+)$ by pooling reaction is unlikely as the energy difference between A and D state (6 eV) is larger than the energy of A state (cf. Fig. 9). A production by electronic impact from the metastable state of N_2 (cf. R2) is also unlikely because: (i) the density of state $A^3\Sigma_u^+$ is in the range of 10^{11}-10^{12} molecules.cm^{-3} (see Ref. 34) and (ii) according to Franck-Condon principle, electronic transitions are promoted between state which inter-molecular distance does not suffer large change, which is not the case of $A^3\Sigma_u^+$ and $D^3\Sigma^+$ state with respectively 1.28656 Å and 1.1081 Å (potential curve is not well known, but r_e was estimated from the relationship given by Lofthus and Krupenie : $r_e(cm^{-1}) = 1.55167786\sqrt{1/B_e}$, with B_e (cm^{-1}) the equilibrium rotational constant, B_e= 1.961 cm^{-1}).[30] On the contrary, X (1.0976968 Å [30]) and D state own similar inter-molecular distance. Hence, the production of $N_2(D^3\Sigma_u^+)$ from the $N_2(X^1\Sigma_g^+)$ by electron-impact excitation appears likely, suggesting an electron population with at least 14 eV. Absolute optical-emission function for the fourth positive system band (0,v'') are given by Filippelli and al.[28]. They found that D-B

Journal of Applied Physics

emission reach a maximum for 14.1±0.3 eV just after the threshold energy and excitation cross section from X(v''=0) to D(v'=0) equal to 1.27×10^{-19} cm^2.

If we assume that electrical characteristics and N_2 concentration are constants, the emission intensity of the fourth positive system remains also constant during the decontamination process. Observation of this system is linked to the NO decrease due to the reactor decontamination. We can conclude that fourth positive system is a good cleanness indicator in pure nitrogen discharge.

Conclusion

In the present paper, contamination by oxygen species was observed in pure nitrogen through the observation of NO-γ in the so called active screen plasma nitriding process operating under pulsed unipolar power supply. This contamination was observed by OES when the discharge is initiated in pure nitrogen immediately after venting the reactor. The temporal evolution of the emission intensity of N_2, N_2^+, NO, OH, H, NH and Fe species was monitored in the spectral range of 200-900 nm. Observation of the fourth positive system of N_2 (only the v' = 0 progression) and NO-γ bands in a N_2 plasmas was reported. To our knowledge, fourth positive system of N_2 was not yet observed in such plasmas applied to nitriding.

It was found that the emission of oxygen containing species (NO and OH) decrease with time, while Fe emission intensity increases with time. Contamination of the reactor surfaces results from water vapour adsorption during reactor venting in order to place the samples to be nitrided. Desorption can be different from the active screen and from the wall, because temperature differences: higher than 500°C on the active screen and around 100°C on the sample placed on the center. The result is a long decay of the NO-γ band emission. After decontamination, the fourth positive system of N_2 could be observed. Such a not commonly observed system can be used as a tool to control reactor cleanness in pure nitrogen discharge

Journal of Applied Physics

AIP Publishing

for nitriding applications. Emission of iron lines consequential to active screen sputtering was found to be correlated to evolution of NO-γ system. This is due to the removal of oxide pollution by ions bombardment of cathodic screen. A way to test the cleanness of the reactor could be to realize pure nitrogen plasma and to verify that NO-γ bands were not observed. Following this test, hydrogen could be introduced in the mixture and treatment begins in a clean atmosphere.

Acknowledgement

This work was performed in the frame of the research project RESEM 2020, managed by the Institut de Recherche Technologique Matériaux Métallurgie Procédés (IRT M2P) and financially supported by the French program Plan d'Investissement d'Avenir (PIA). We acknowledge G. Cernogora of LATMOS laboratory, Université de Versaille Saint Quentin en Yvelines, for his help in understanding the population mechanism of $N_2(D^3\Sigma_u^+)$.

Data availability

The data that support the findings of this study are available from the corresponding author upon reasonable request.

Reference

[1]S. Li, J.A.M. Jimenez, V. Hessel and F. Gallucci, Processes 20, 248 (2018).

[2]P. Peng, C. Schiappacasse, N. Zhou, M. Addy, Y. Cheng, Y. Zhang, K. Ding, Y. Wang, P. Chen, and R. Ruan, ChemSusChem 12**,** 3702 (2019).

[3]L. Lin, H. Xu, H. Gao, X. Zhu, and V. Hessel, J. Phys. D: Appl. Phys. 53 133001 (2020).

[4]E. Rolinski 2014 Plasma assisted nitriding and nitrocarburizing of steel and other ferrous alloys *Thermochemical Surface Engineering of Steels* ed. E J Mittemeijer and M A J Somers, Pub. Woodhead Publishing 413.

[5]A. Pavlik, G. Marcos, M. Coulibaly, M. Vincent, T. Czerwiec, and T. Philippon, Tribol. Int 146, 106232 (2020).

[6]T. Czerwiec, H. Michel, and E. Bergmann , Surf. Coat. Technol. 108-109, 182 (1998).

[7]J-P. Lebrun, Proc. 10th Int. Congr. IFHTSE 169, (1996).

[8]Georges J *US Patent* 5,989,363. Nov. 1999.

[9]Georges J *Proc. 12th Congr. IFHTSE* 229.

[10] H-J. Spies, I. Burlacov, K. Borner, and H. Biermann, Int. Heat Treatment and Surface Engineering 8**,** 1 (2014).

[11]C.X. Li, Surf. Eng. 26, 135 (2010).

[12]S.C. Gallo, and H. Dong, Surf. Coat. Technol. 203, 3669 (2009).

[13]I. Burlacov, K. Börner, H-J. Spies, H. Biermann, D. Lopatik, H. Zimmermann, and J. Röpcke, Surf. Coat. Technol. 206, 3955 (2012).

[14]D. Kovács, J. Dobránszky, and A. Bonyár, Results Phys. 12, 1311 (2019).

[15]A. Nishimoto, K. Nagatsuka, R. Narita, H. Nii, and K. Akamatsu, J. ASTM Int. 8, 1 (2011).

[16]A. Itoh, Y. Ishikawa, and Y. Kawabe, J. Vac. Sci. Technol. A 6, 2421 (1988).

[17]Y.H. Shin, K.J. Lee, and K.H. Chung Jhung, Vacuum 47, 679 (1996).

[18]D. Kovács, J. Dobránszky, T. Fodor, V. Takáts, and A. Bonyár, Surf. Coat. Technol. 394, 125638 (2020).

[19]D.L. Crintea, U. Czarnetzki, S. Iordanova, I. Koleva, and D. Luggenhölscher, J. Phys. D: App. Phys. 42, 045208 (2009).

[20]J. Walkowicz, Surf. Coat. Technol. 174-175, 1211 (2003).

[21]K.S. Suraj, P. Bharathi, V. Prahald, and S. Mukherjee, Surf. Coat. Technol. 202, 301 (2007).

[22]L. Petitjean, and A. Ricard, J. Phys. D.: Appl. Phys. 17, 919 (1984).

[23]M. Hannemann, S. Hamann, I. Burlacov, K. Börner, H-J. Spies, and J. Röpcke, Surf. Coat. Technol. 235, 561 (2013).

[24]S. Hamann, K. Börner, I. Burlacov, H-J. Spies, and J. Röpcke, J. Phys. D: App. Phys. 48, 345204 (2015).

[25]H. Michel, T. Czerwiec, M. Gantois, D. Ablitzer, and A. Ricard, Surf. Coat. Technol. 72, 103 (1995).

[26]H. Uyama, and O. Matsumoto, Plasma Chem. Plasma Process. 9, 13 (1989).

[27]O. Matsumoto, M. Konuma, and Y. Kanzaki, J. Less Common Met. 84, 157 (1982).

[28]A.R. Filippelli, S. Chung, and C. Lin Chun, Phys. Rev. A 29, 1709 (1984).

[29]B.R. Lewis, K.G.H Baldwin, A.N. Heays, S.T. Gibson, J.P. Sprengers, W. Ubachs, and M. Fujitake, J. Chem. Phys 129, 204303 (2008).

[30]A. Lofthus, and P.H. Krupenie, J. Phys. Chem. Ref. Data 6, 113 (1977).

[31]Y. Ishikawa, and T. Yoshimura, J. Vac. Sci. Technol. A 13, 1847 (1995) .

[32]J.P. Joly, F. Gaillard, E. Peillex, and M. Romand, Vacuum 59, 854 (2000).

[33]T. Czerwiec, K. Anoun, M. Remy, and H. Michel, Mater. Sci. Eng. A 139, 276 (1991).

[34]Ricard A 1995 *Plasma reactifs* Ed. SFV.

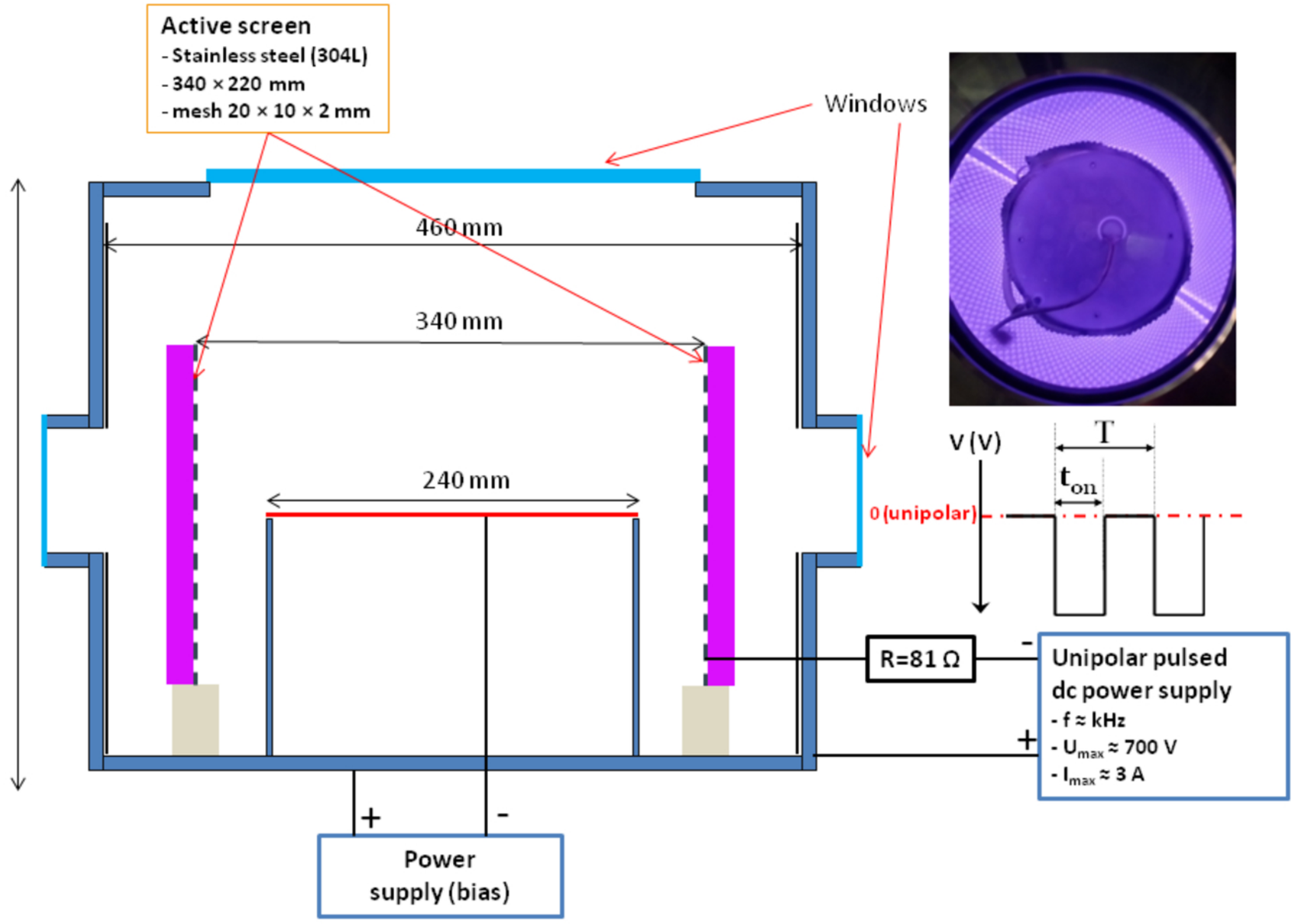

AIP Publishing

Journal of Applied Physics

ACCEPTED MANUSCRIPT

This is the author's peer reviewed, accepted manuscript. However, the online version of record will be different from this version once it has been copyedited and typeset.
PLEASE CITE THIS ARTICLE AS DOI: 10.1063/5.0064704

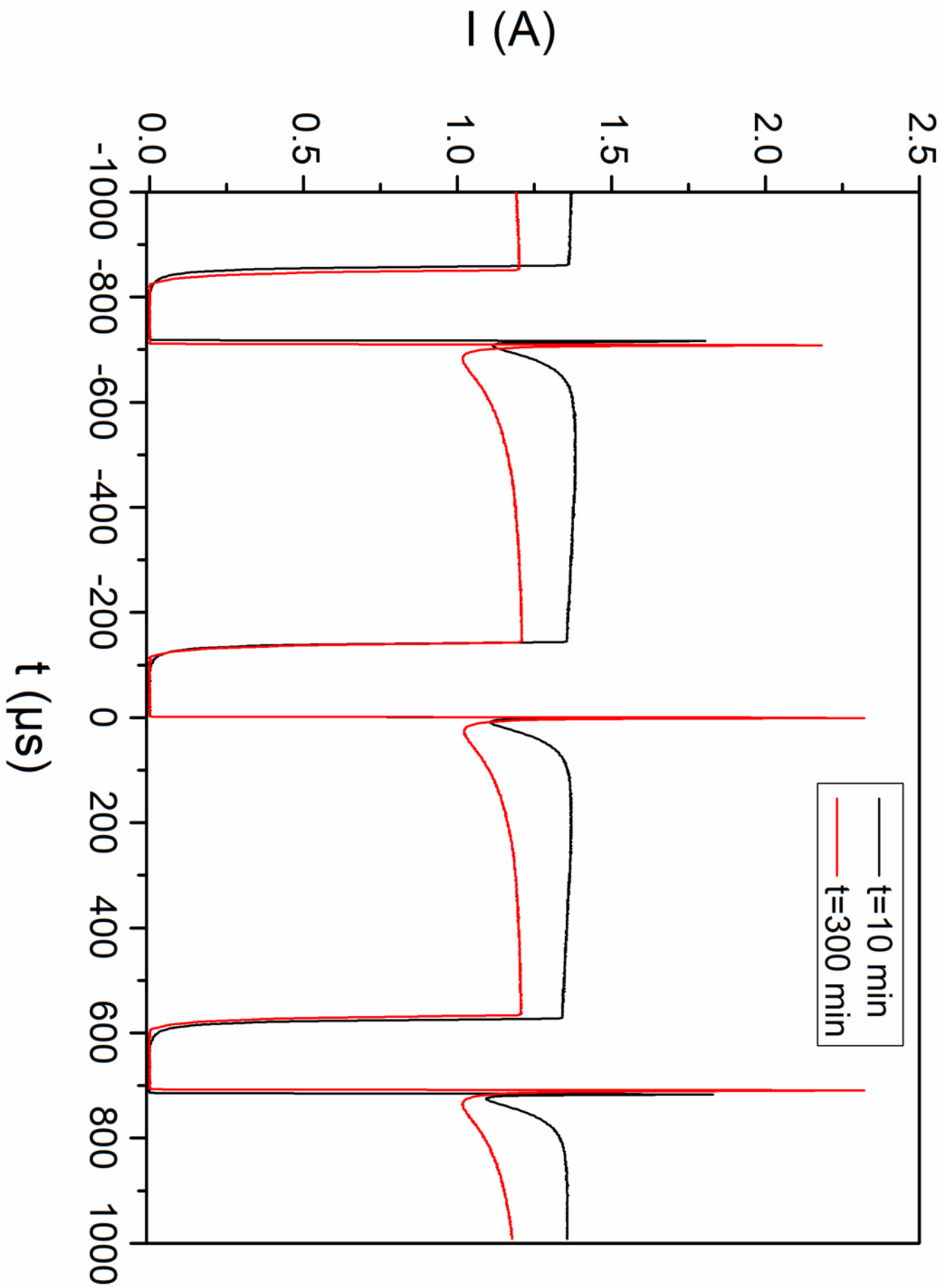

Journal of Applied Physics

PLEASE CITE THIS ARTICLE AS DOI: 10.1063/5.0064704

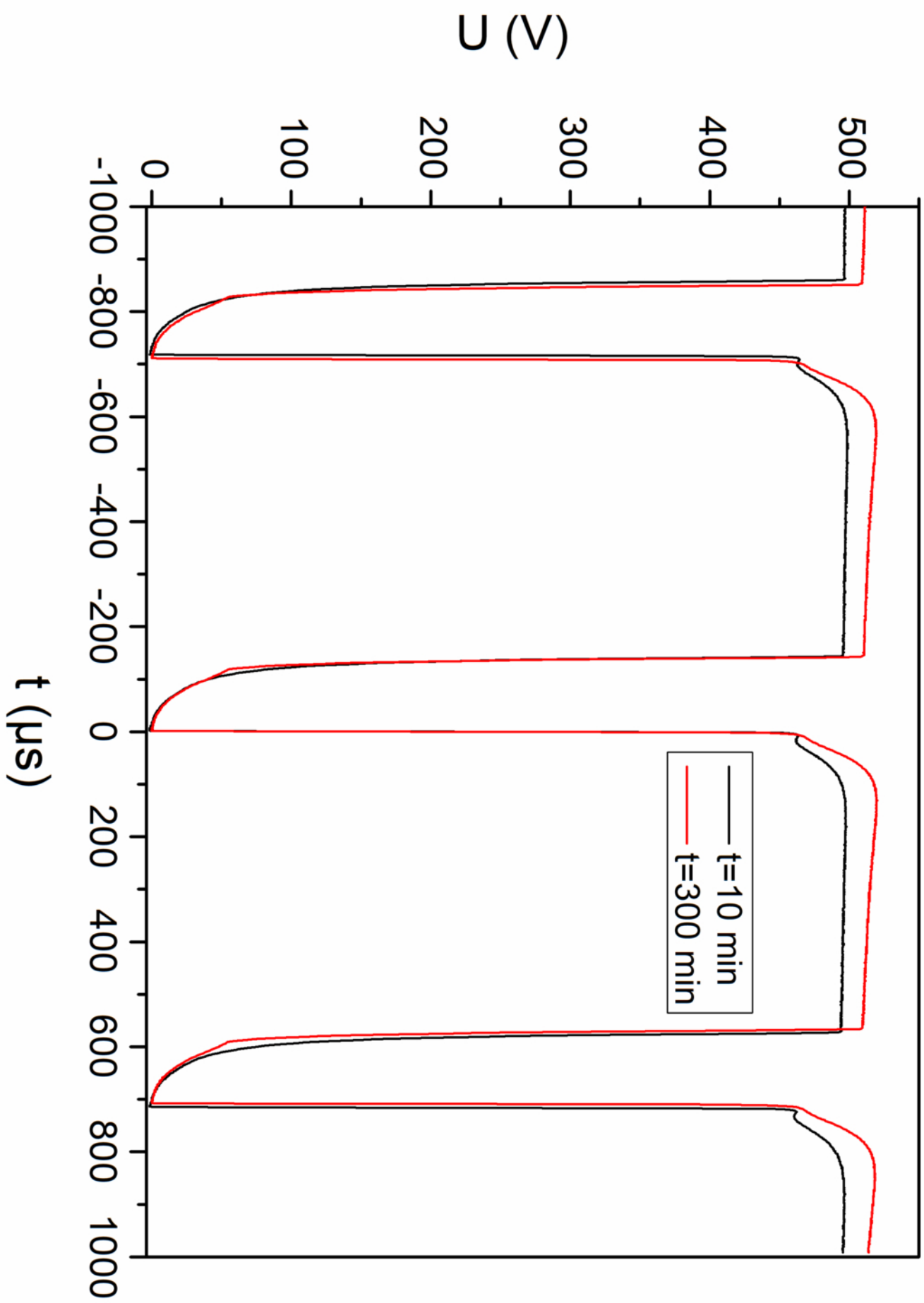

AIP Publishing

Journal of Applied Physics

ACCEPTED MANUSCRIPT

This is the author's peer reviewed, accepted manuscript. However, the online version of record will be different from this version once it has been copyedited and typeset.
PLEASE CITE THIS ARTICLE AS DOI: 10.1063/5.0064704

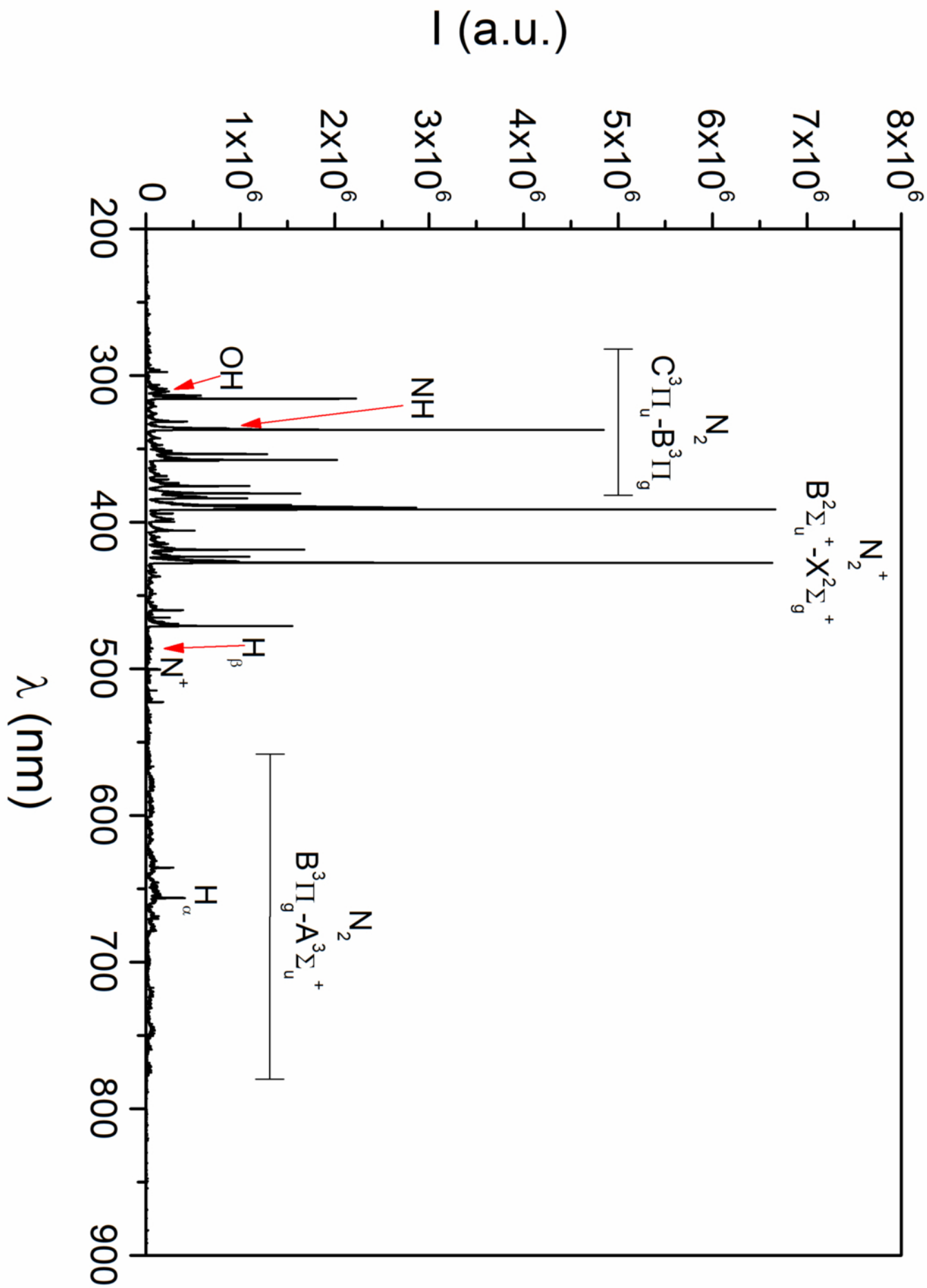

AIP Publishing

Journal of Applied Physics

ACCEPTED MANUSCRIPT

This is the author's peer reviewed, accepted manuscript. However, the online version of record will be different from this version once it has been copyedited and typeset.
PLEASE CITE THIS ARTICLE AS DOI: 10.1063/5.0084704

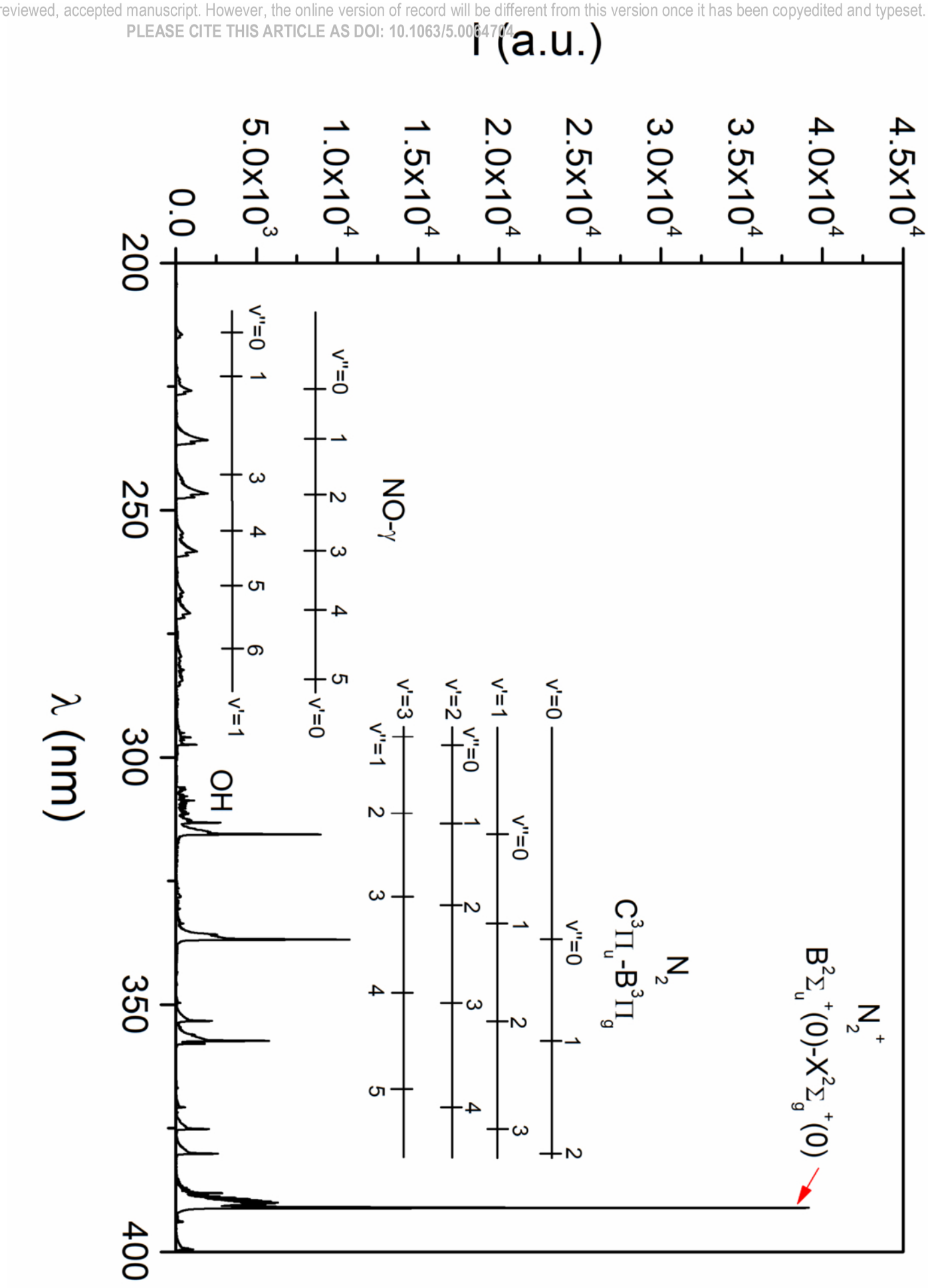

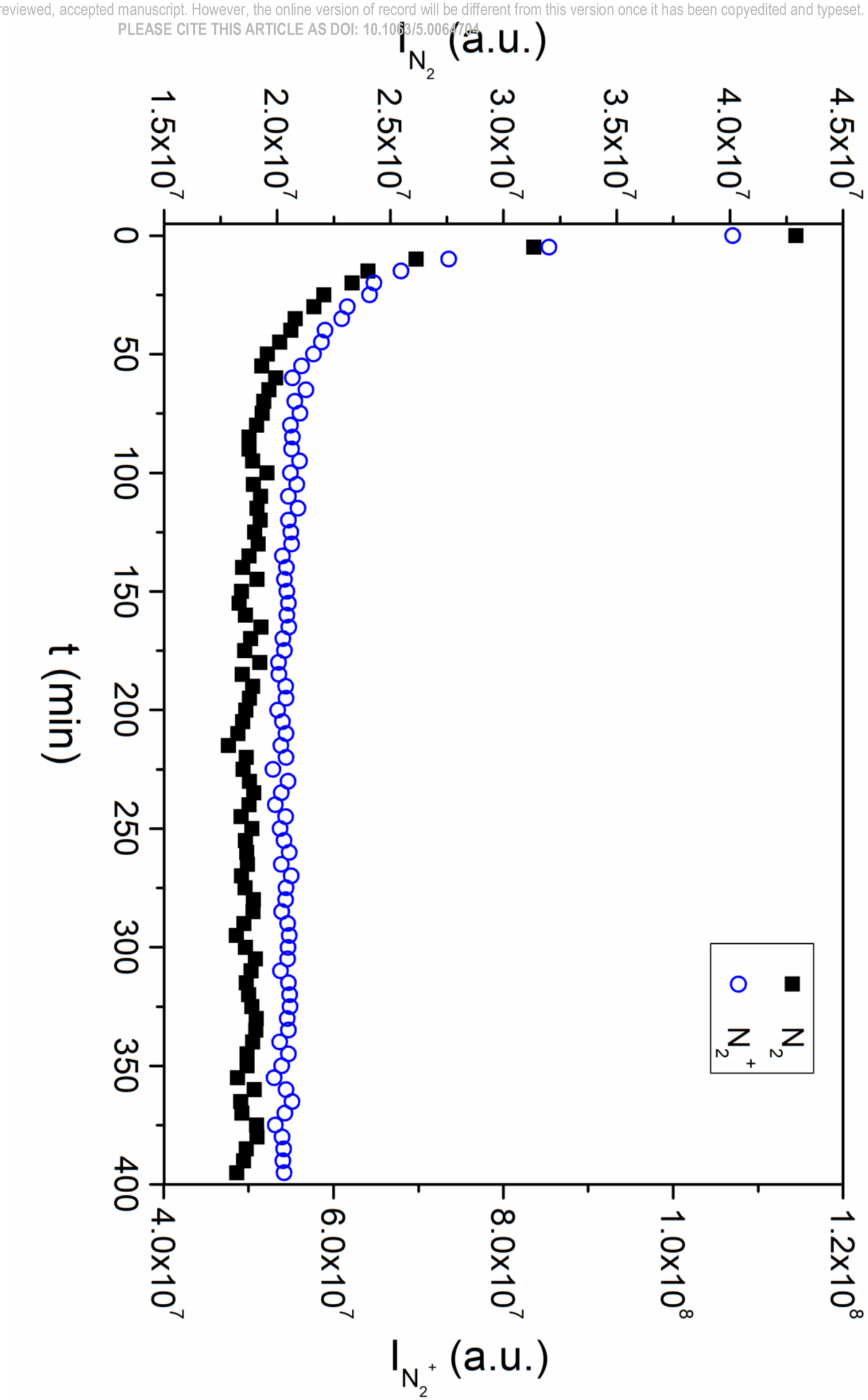

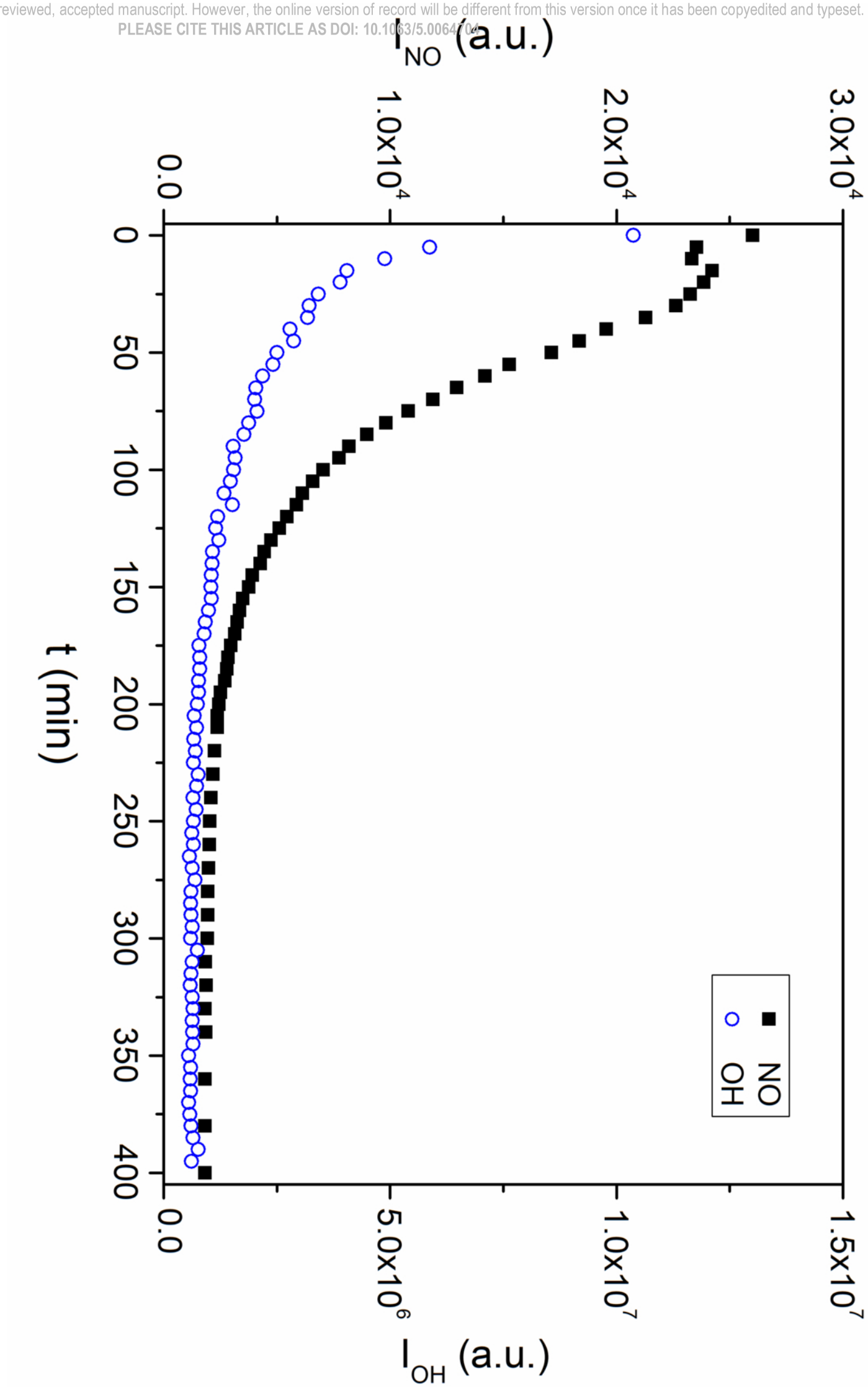

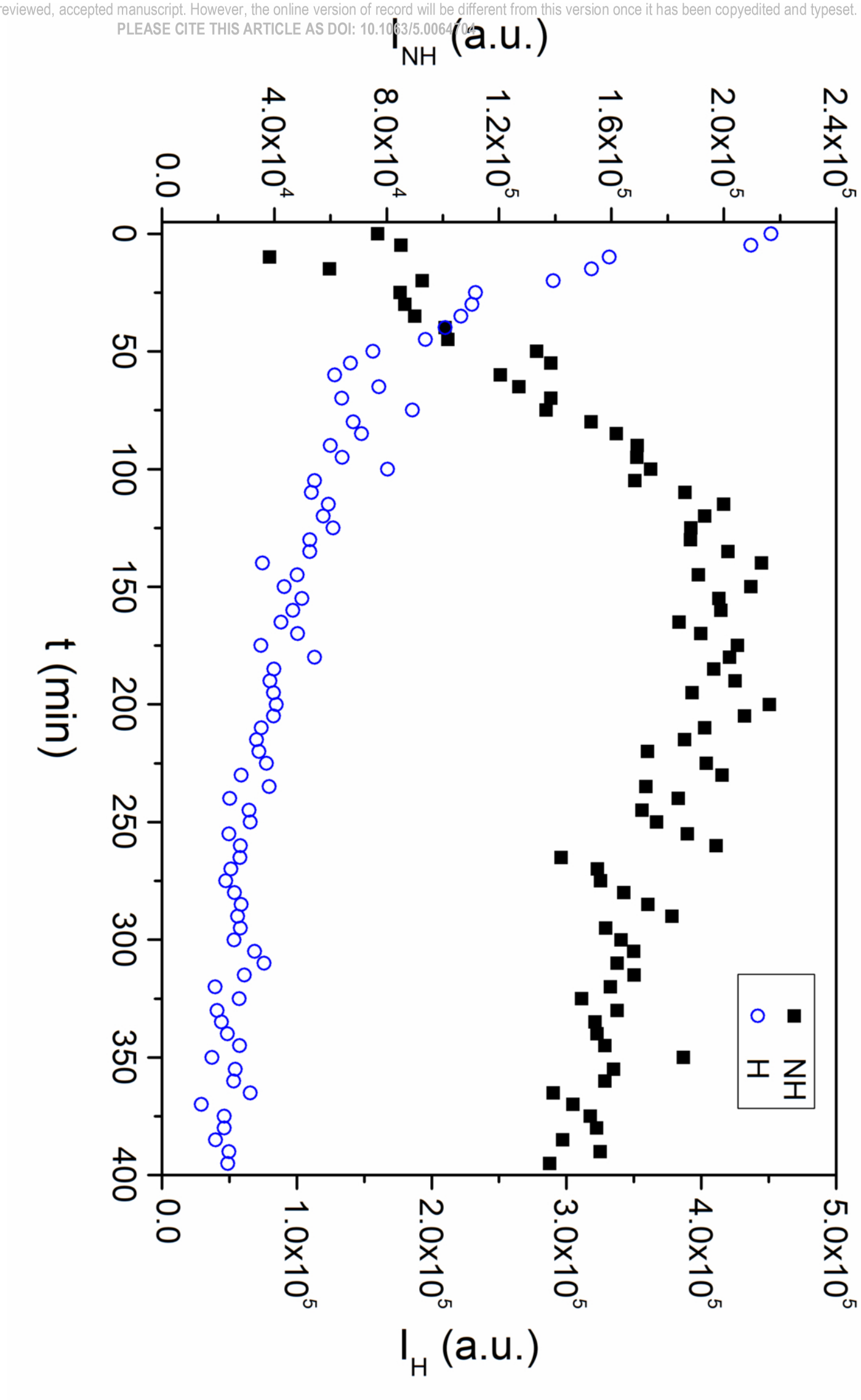

Journal of Applied Physics

PLEASE CITE THIS ARTICLE AS DOI: 10.1063/5.0064704

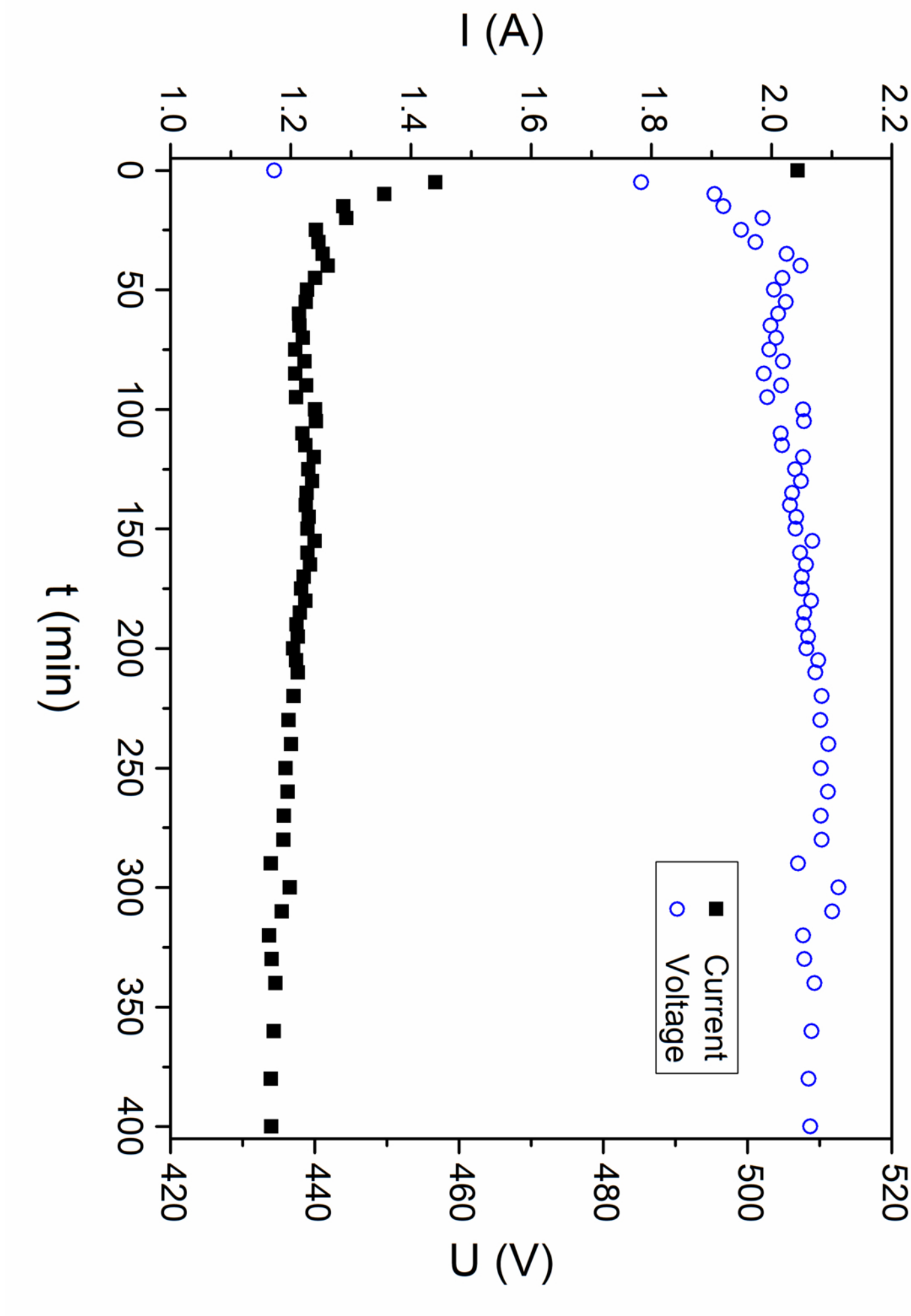

Journal of Applied Physics

PLEASE CITE THIS ARTICLE AS DOI: 10.1063/5.0064704

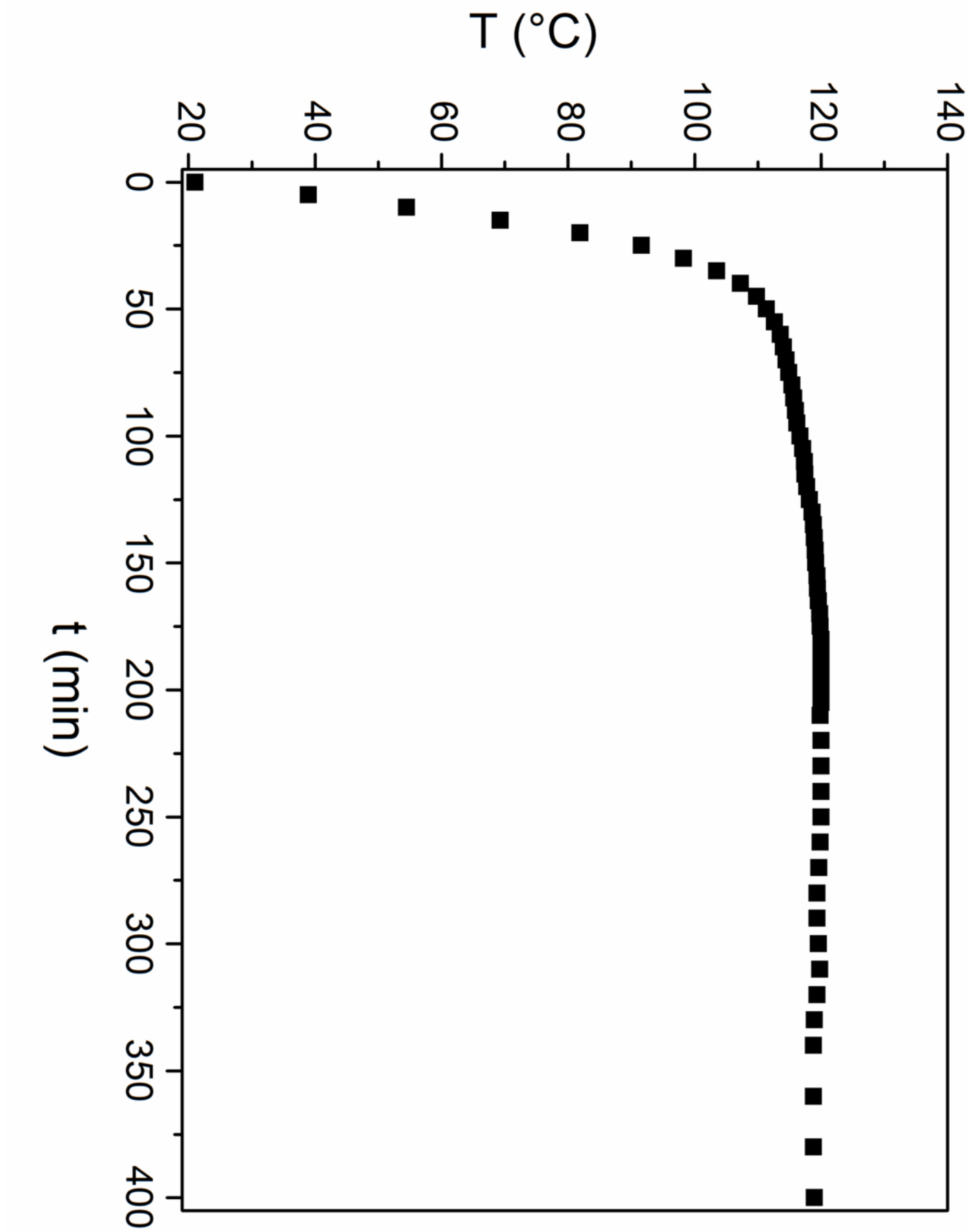

Journal of Applied Physics

PLEASE CITE THIS ARTICLE AS DOI: 10.1063/5.0064704

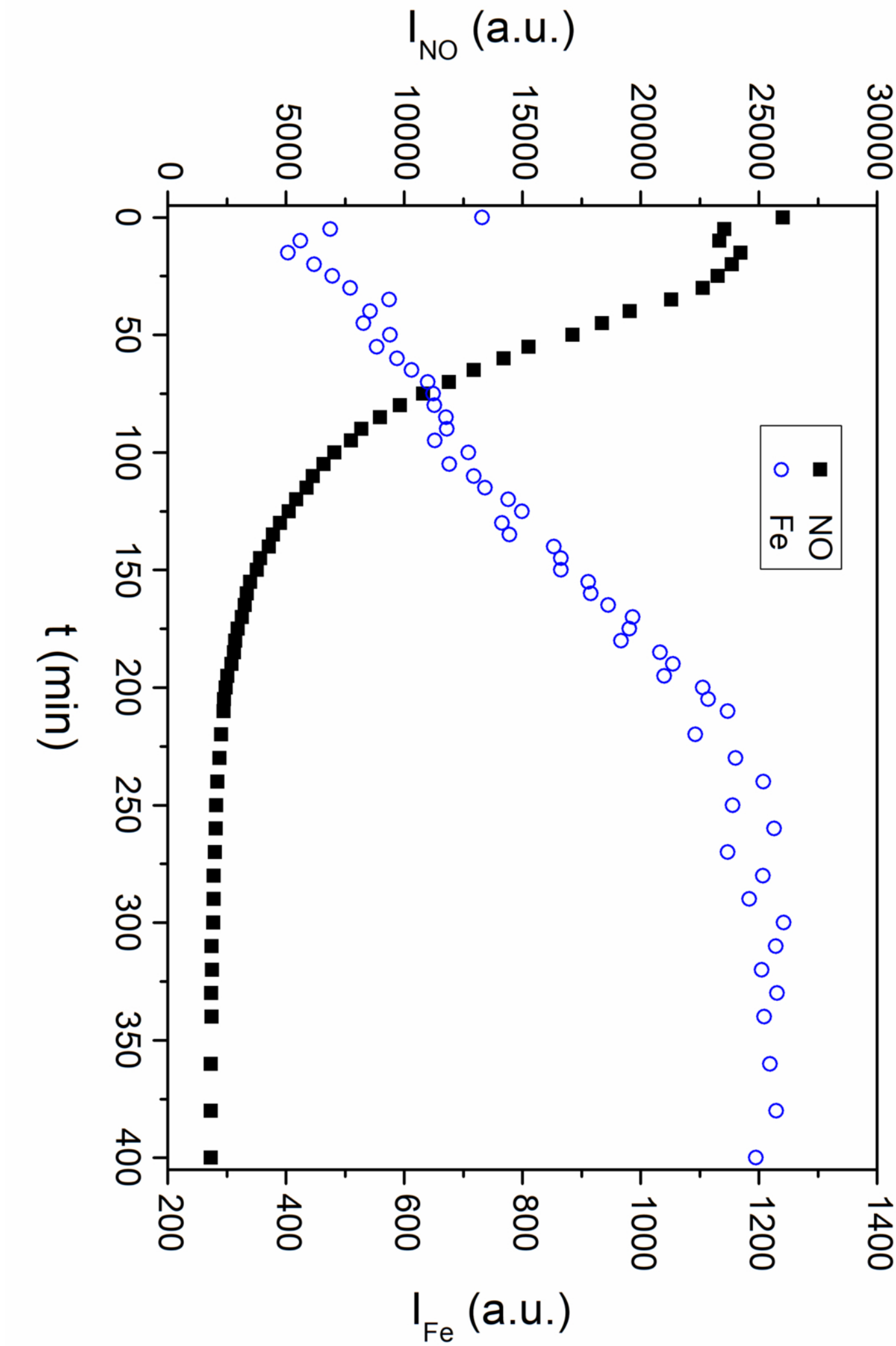

AIP Publishing

Journal of Applied Physics

ACCEPTED MANUSCRIPT

This is the author's peer reviewed, accepted manuscript. However, the online version of record will be different from this version once it has been copyedited and typeset.
PLEASE CITE THIS ARTICLE AS DOI: 10.1063/5.0064704

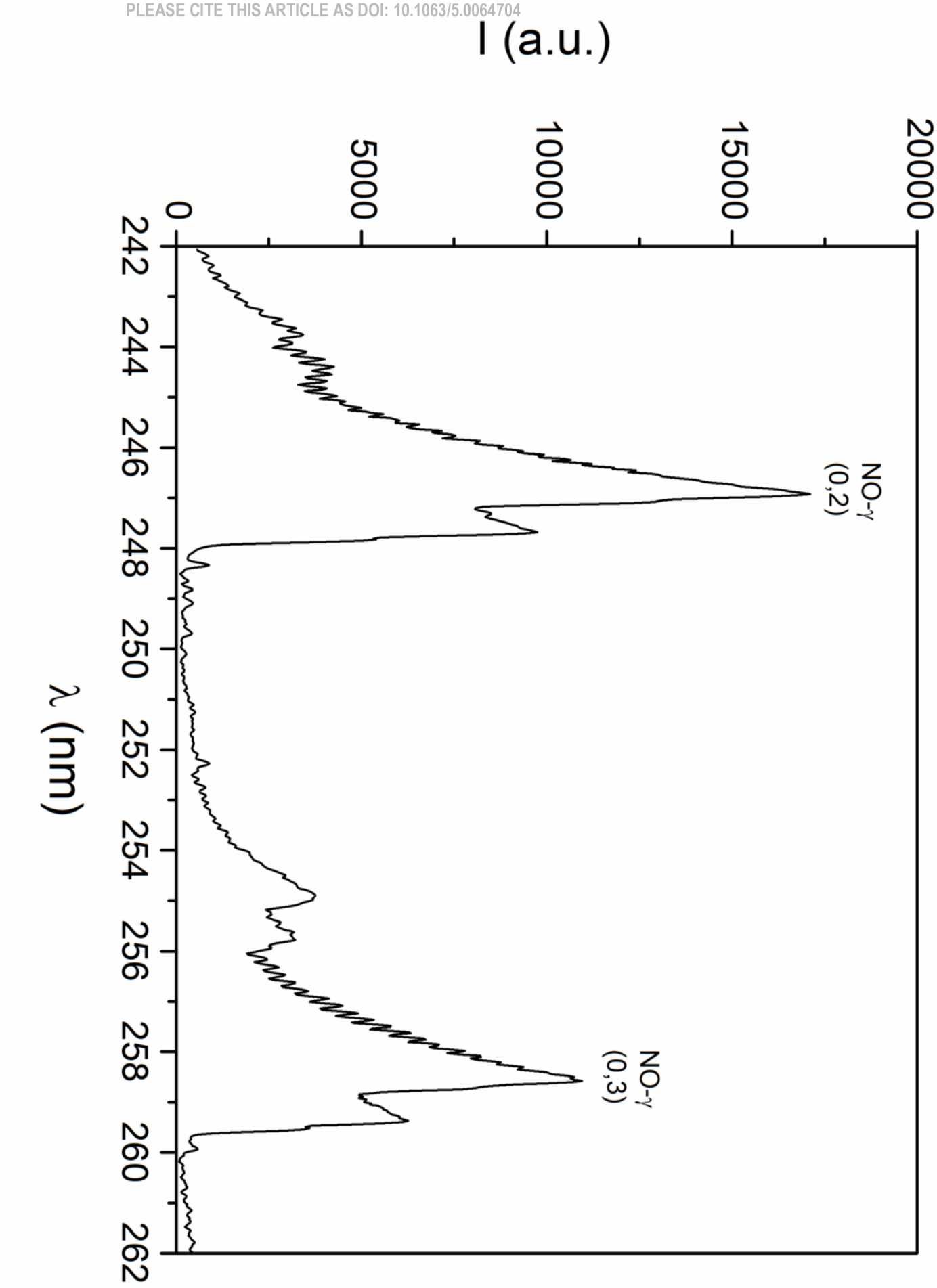

AIP Publishing

Journal of Applied Physics

ACCEPTED MANUSCRIPT

This is the author's peer reviewed, accepted manuscript. However, the online version of record will be different from this version once it has been copyedited and typeset.
PLEASE CITE THIS ARTICLE AS DOI: 10.1063/5.0064704

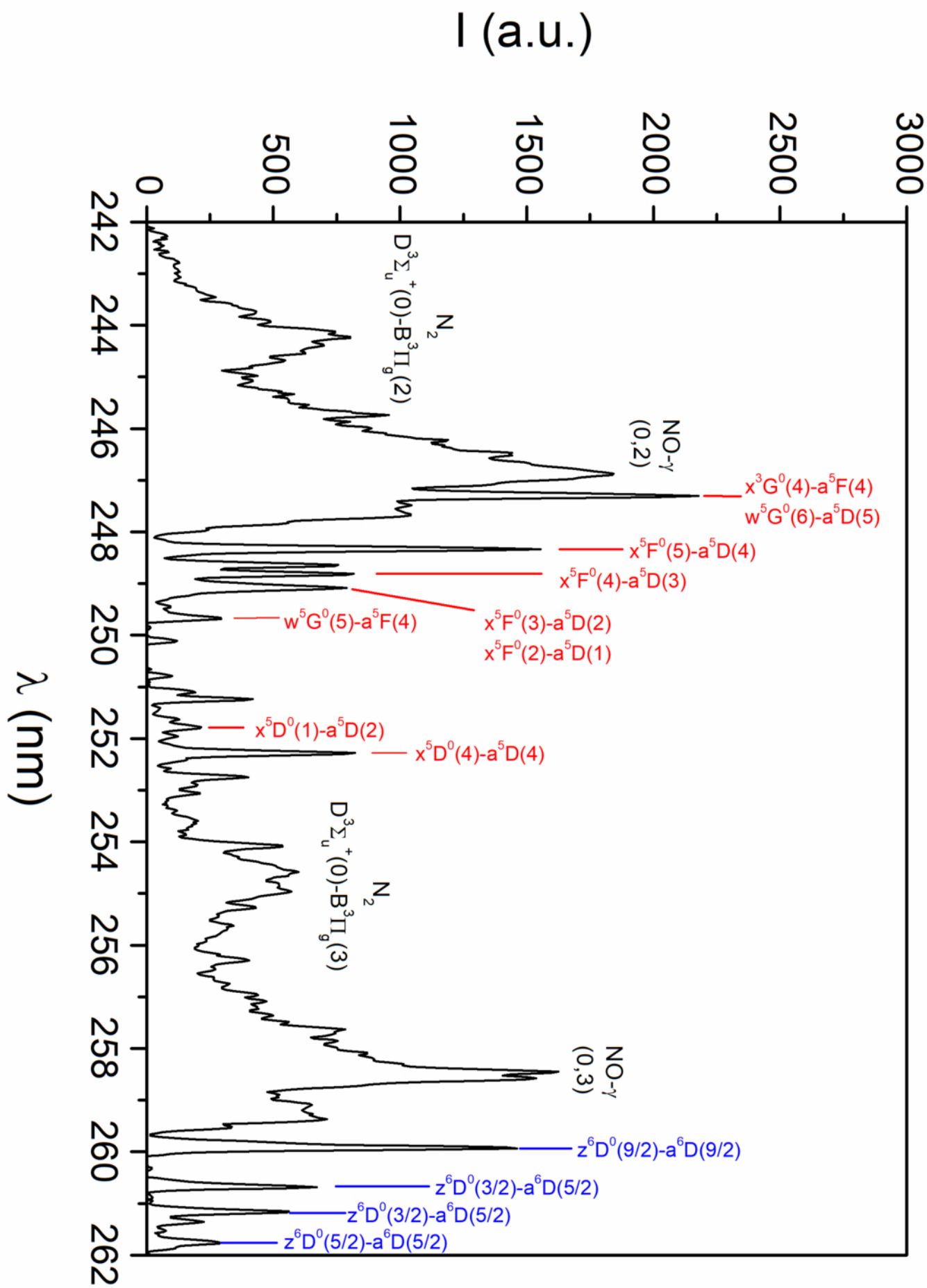

AIP Publishing

Journal of Applied Physics

ACCEPTED MANUSCRIPT

This is the author's peer reviewed, accepted manuscript. However, the online version of record will be different from this version once it has been copyedited and typeset.
PLEASE CITE THIS ARTICLE AS DOI: 10.1063/5.0064704

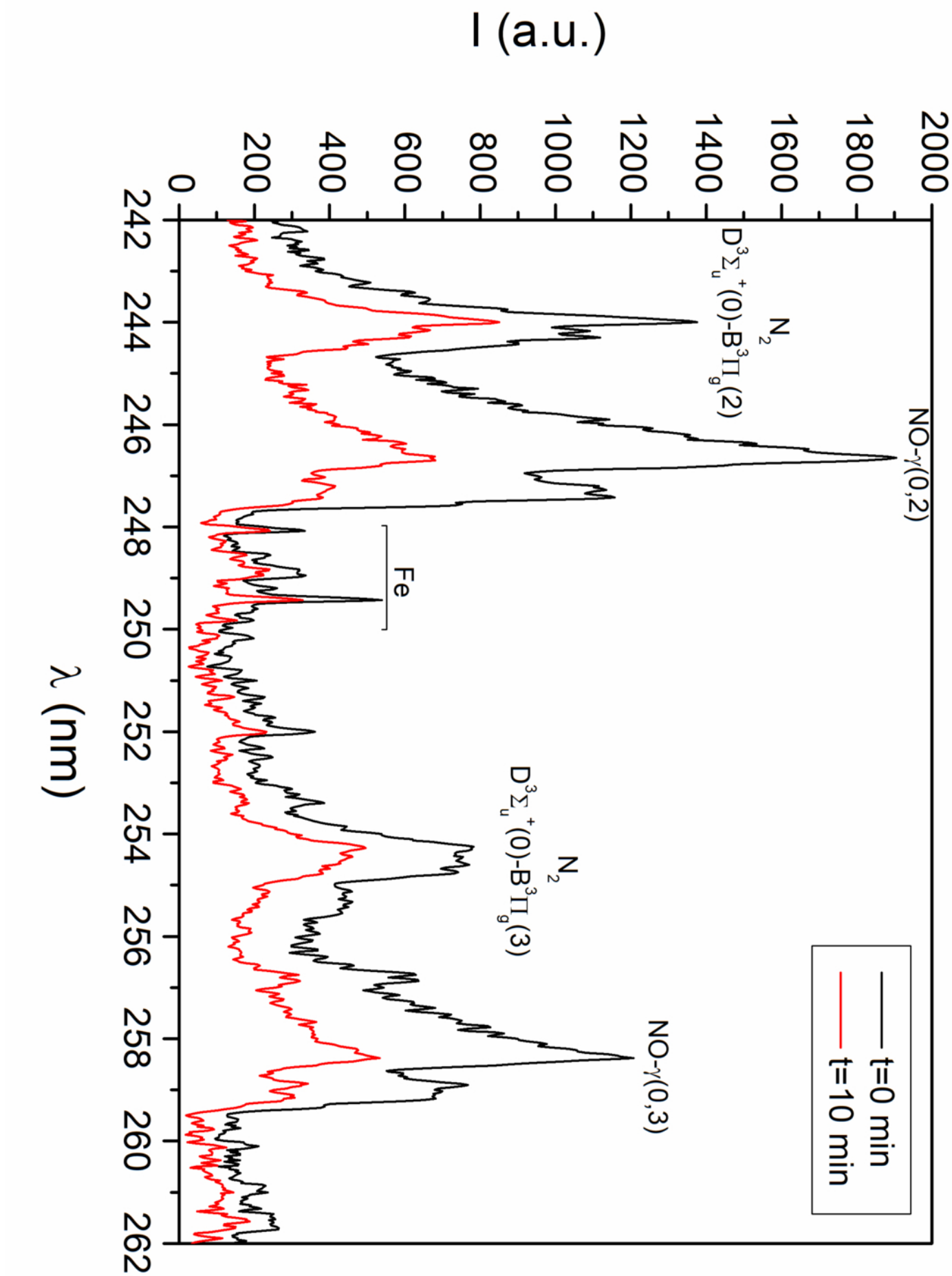

AIP Publishing

Journal of Applied Physics

ACCEPTED MANUSCRIPT

This is the author's peer reviewed, accepted manuscript. However, the online version of record will be different from this version once it has been copyedited and typeset.
PLEASE CITE THIS ARTICLE AS DOI: 10.1063/5.0064704

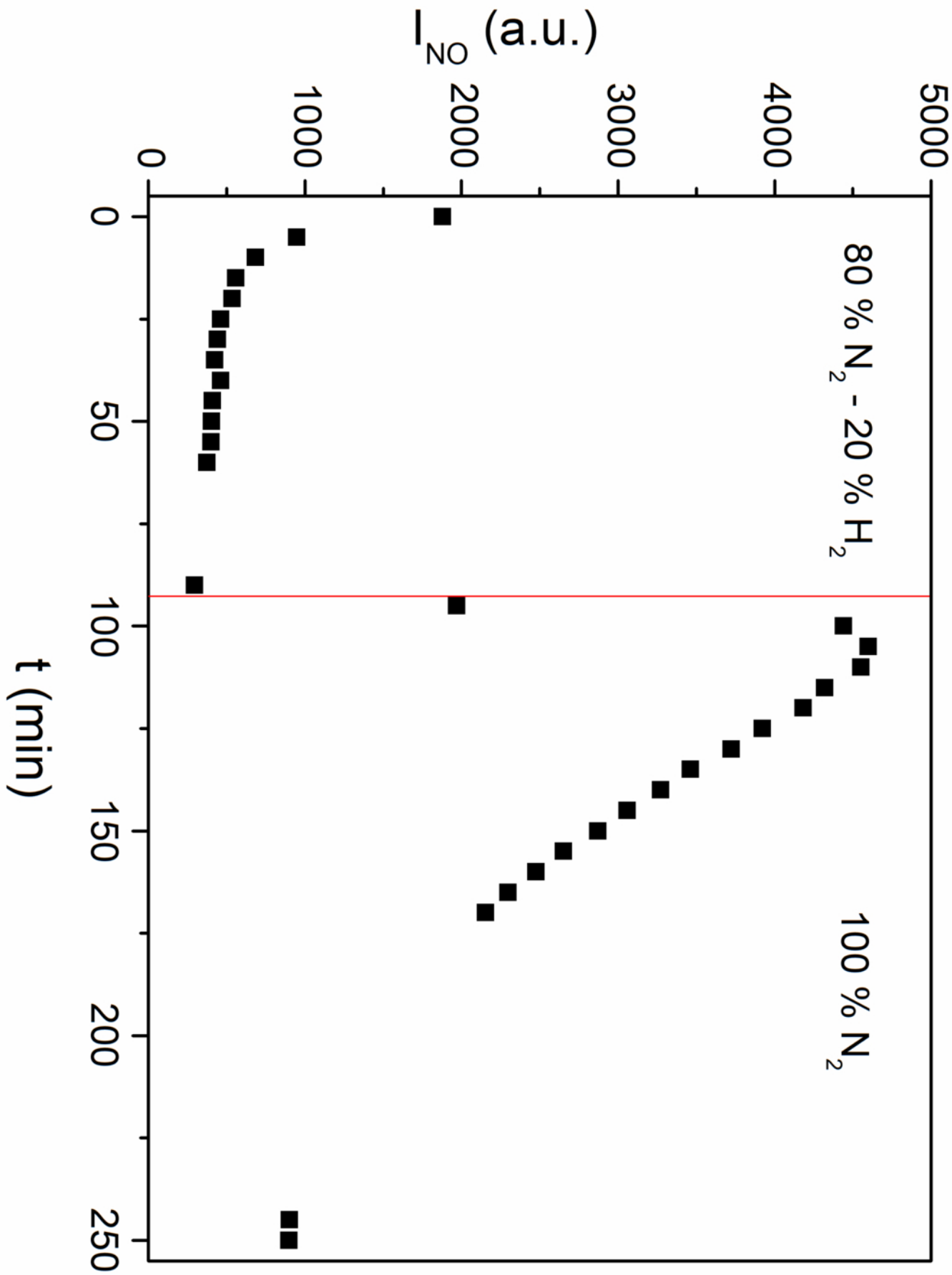

Journal of Applied Physics

PLEASE CITE THIS ARTICLE AS DOI: 10.1063/5.0064704